

# Dimension Reduction and Identification of Dynamic Barriers in Structural Transitions of Clusters \*

Tomohiro Yanao

*Fukui Institute for Fundamental Chemistry, Kyoto University, Kyoto 606-8108, Japan*

e-mail: yanao@fukui.kyoto-u.ac.jp

## Abstract

This report highlights the author's recent study with W. S. Koon (Caltech), J. E. Marsden (Caltech), and I. G. Kevrekidis (Princeton University). Molecular reactions as well as functional motions of biopolymers are typically large-amplitude collective motions that involve a large number of degrees of freedom in a coherent manner. It has been a significant challenge to understand the mechanism for such collective motions. By taking up a six-atom cluster as an illustrative example, we develop a methodology to understand collective motions of molecules with many degrees of freedom in terms of the reduced dynamics of gyration radii, which serve as predominant collective variables. We highlight the competition between two different kinds of forces that essentially mediate the dynamics of gyration radii: One is the ordinary potential force that originates from the potential energy function of the system, and the other is an internal centrifugal force that originates from the intrinsic non-Euclidean nature of molecular internal space. While the potential force generally works to keep the mass distribution of the system compact and symmetric, the internal centrifugal force works to inflate and elongate it. We show that the internal centrifugal force induces a significant dynamic barrier for reaction, which can often overshadow the original potential energy barrier. This kind of geometry-related dynamical effects should shed new light on the conventional picture of molecular reactions.

## 1 Introduction

Large-amplitude collective motions play an essential role in chemical reactions as well as in the functional motions of biomolecules. Understanding the mechanism for such collective motions has been a significant challenge in current molecular science. Since such collective motions involve a large number of degrees of freedom in a coherent manner, reducing the dimensionality by using a small number of appropriate collective variables

---

\*Based on the paper, T. Yanao, W. S. Koon, J. E. Marsden, and I. G. Kevrekidis, *J. Chem. Phys.* **126**, 124102 (2007).

is crucially important. Indeed, dimensionality reduction has been a long-standing issue in nonequilibrium statistical mechanics [1–3], molecular dynamics [4–6], Monte Carlo methods [7], and in reaction path theories [8–10].

The first issue of this report is to find out appropriate collective variables (or equivalently reaction coordinates) that play predominant roles rather ubiquitously in a wide class of large-amplitude motions of molecular systems. We specifically highlight the three *gyration radii* of a molecule as such collective variables in this study. Physically, the gyration radii are the measure of mass distribution of a system along the three principal axes. We investigate the three-dimensional dynamics of gyration radii of a general  $n$ -atom molecule both analytically and numerically at the level of their classical equations of motion. To this end, we first reduce the three translational and three rotational degrees of freedom from the  $3n$  total degrees of freedom configuration space correctly using the framework of standard reduction theory for symmetric systems following [11, 12] and the gauge theory [13–19]. In order to carry out further reduction in dimensions, beyond symmetry reduction, we employ the principal-axis hyperspherical formalism, which was initiated in an early paper by Eckart [20] and reformulated in the hyperspherical context by Chapuisat *et al.* [21, 22] and Kuppermann [23–25].

In the principal-axis hyperspherical formalism, the instantaneous principal axes of the system are used as a body frame. Then the  $(3n - 6)$  internal degrees of freedom are parametrized by the three gyration radii and the  $(3n - 9)$  hyperangles. While the gyration radii characterize the mass distribution of the system, hyperangles are associated with cyclic and democratic deformation of the system called kinematic rotation, which was scrutinized by Littlejohn *et al.* [26–28] and Aquilanti *et al.* [29–31]. It was shown in Refs. [20–22] that the use of  $(3n - 9)$  quasivelocities instead of the hyperangles simplifies the expression of kinetic energy of  $n$ -body systems remarkably. By taking the advantage of this concise expression for kinetic energy, we here derive classical equations of motion, which are also concise and physically appealing.

In the present study, the three gyration radii are regarded as slow collective variables that essentially dominate large-amplitude motions of the system, while the hyperangular variables are regarded as fast “bath” modes. This distinction of variables is based mainly on time scale separation and kinetic energy partitioning as will be shown in this report. Based on this classification of the variables, we average out the hyperangular variables that appear in the equations of motion for the gyration radii to obtain a set of approximately closed equations of motion for the gyration radii.

The averaged equations of motion for the gyration radii shed light on the mechanism of competition between the potential force and a dynamic force in large-amplitude motions of polyatomic molecules. The dynamic force has its origin in the kinematic coupling of gyration radii with the hyperangular modes (kinematic rotations) via the non-Euclidean metric of the internal space. This dynamic force is essentially an *internal centrifugal force* arising from the internal motions themselves. Generally speaking, the potential force works to keep the internal mass distribution of a molecule symmetric and compact. On the other hand, the internal centrifugal force has the remarkable effect of elongating and inflating the internal mass distribution of the molecule. In other words, the molecular vibrations induce a spontaneous tendency of deformation. In this way, the internal centrifugal force can be the critical driving force for a molecule to move from one potential

well to another. We show that this dynamic force induces a significant dynamic barrier for reaction, which can often overshadow the original potential energy barrier. The effects of the internal centrifugal force in three-atom and four-atom reactions have been studied in Refs. [32–34]. In this report, we present a generalized method of these results to larger  $n$ -atom molecules involving systematic averaging based on our recent publication [35].

As an illustrative example, we take up the structural transition dynamics of a six-atom Morse cluster, which represents an  $\text{Ar}_6$ -like cluster [36–38], with constant energy and with zero total angular momentum. The cluster possesses two kinds of geometrically distinct isomers, one of which has a regular octahedron structure, which is highly symmetric, and the other has a elongated structure. The octahedron structure lies at the bottom of a much deeper potential well. Interestingly, this cluster shows a clear switching of structural preference depending on its total energy. In the low energy range (solid-like phase), the cluster spends more time in the potential well of the octahedron structure, while in the high energy range (liquid-like phase), the cluster spends more time in the competing potential well. This kind of two-state switching is a general feature of the first-order phase transitions as is observed in larger clusters [39–41] and proteins [42, 43]. We will provide a novel explanation for such switching in terms of the competition between the potential force and the internal centrifugal force.

This report is organized as follows. In Sec. 2, after introducing the model system, the six-atom Morse cluster, we present how the structural transition dynamics of the cluster is coarsely characterized by the gyration radii. In Sec. 3, we introduce the principal-axis hyperspherical coordinates, and derive general equations of motion for the gyration radii of isolated  $n$ -atom systems. By averaging these equations of motion for the gyration radii, the competition between a kinematic force and the potential force is characterized in Sec. 4. Mechanism of switching of structural preference of the cluster is explained in terms of a dynamic barrier. The report concludes in Sec. 5 with some remarks regarding future studies.

## 2 Collective Variables in Structural Transition Dynamics of Clusters

### 2.1 Model cluster and residence probabilities

We first introduce our prototypical model for the study of molecular conformational transitions; an atomic cluster composed of six identical atoms that mutually interact through the pairwise Morse potential. This is called an  $\text{M}_6$  cluster. The dimensionless Hamiltonian of the system is given by

$$\frac{\mathcal{H}}{\varepsilon} = \frac{1}{2} \sum_{i=1}^6 (\dot{\mathbf{r}}_{si} \cdot \dot{\mathbf{r}}_{si}) + \sum_{i<j} [e^{-2(d_{ij}-d_0)} - 2e^{-(d_{ij}-d_0)}], \quad (1)$$

where  $\mathbf{r}_{si}$  ( $i = 1, \dots, 6$ ) is the three-dimensional position vector of the atom  $i$ . The subscript  $s$  represents the quantity with respect to the space-fixed frame. (This rule is also applied to other quantities.) The dot over  $\mathbf{r}_{si}$  represents the time derivative. All the

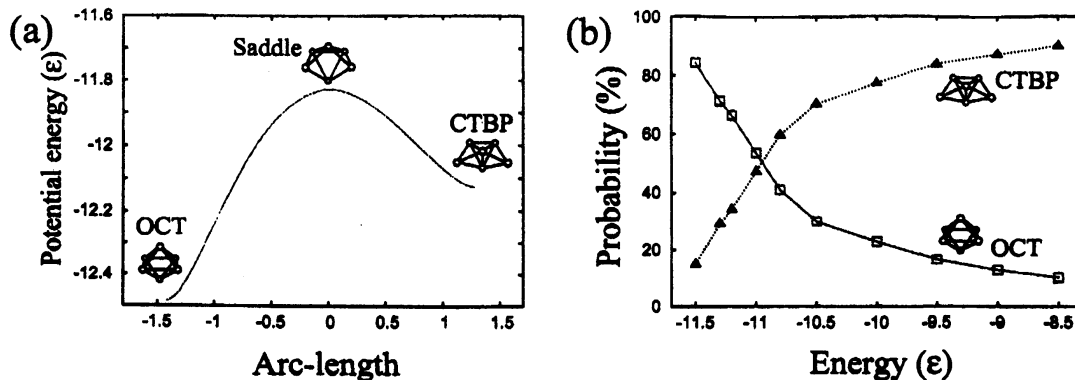


Figure 1: (a) Isomerization scheme of the six-atom Morse cluster. The cluster has two geometrically distinct isomers, OCT and CTBP. The potential energy curve along the steepest descent path connecting the saddle point and the two potential minima is shown. (b) Energy dependence of the residence probabilities of the  $M_6$  cluster in the two isomers. Open squares represent the residence probability for the OCT isomer, while the open triangles represent the residence probability for the CTBP isomer.

masses of the atoms are set to unity,  $m_i = 1$  ( $i = 1, \dots, 6$ ). The parameter  $\epsilon$  represents the depth of the Morse potential and  $d_{ij}$  is the inter-particle distance between atom  $i$  and atom  $j$ . The parameter  $d_0$ , which corresponds to the equilibrium distance of the pairwise Morse potential, is set to  $d_0 = 6.0$ . This provides a potential topography similar to that of the Lennard-Jones potential [37]. Therefore, this system can be regarded as a model of the  $Ar_6$  cluster. Since the main interest of this study is in the internal dynamics of polyatomic systems, the total angular momentum of the system is assumed to be zero throughout the report. In what follows, our numerical results are presented in absolute units.

The isomerization (structural transition) scheme of the  $M_6$  cluster is shown in Fig. 1(a). This cluster has two geometrically distinct isomers: One is the regular octahedron (OCT) and the other is the capped trigonal bipyramid (CTBP) [36–38]. The potential energy minimum of the OCT isomer is  $V = -12.49\epsilon$ , and that of the CTBP isomer is  $V = -12.13\epsilon$ . These two isomers are connected through a saddle point whose potential energy is  $V = -11.83\epsilon$ . In Fig. 1(a), the potential energy topography along the steepest descent path is shown. The horizontal axis is the arc-length of the path in the space of gyration radii, which will be introduced later. Note that the OCT isomer has a highly symmetric spherical structure with a deep potential well, while the CTBP isomer has an elongated (collapsed) structure with a shallow potential well.

In this study, we employ a microcanonical, constant energy simulation. When the total energy of the cluster is higher than that of the saddle point, the isomerization reaction between the two isomers is energetically possible. Occurrence of the structural isomerization reaction is detected by the quenching method [36], which solves the first order equations,  $dr_{si}/d\tau = -\partial V/\partial r_{si}$ , at each instant until the system arrives at one of the minima on the potential energy surface. The parameter  $\tau$  is arbitrary. With this method, every point along a classical trajectory is attributed to one of the two isomers

except for the saddle points.

Fig. 1(b) shows the energy dependence of the percentages of the total residence times in the two isomer wells obtained through a long-time simulation. These are essentially the probabilities of finding the system in the respective configurations. In the low energy range, the  $M_6$  cluster spends more time in the OCT isomer than in the CTBP isomer. This is understandable from the view point of the potential energy topography since the potential well of the OCT isomer is much deeper than that of CTBP as shown in Fig. 1(a). However, as energy increases, the structural preference of the cluster switches dramatically, and the system prefers to be in the CTBP isomer than in the OCT. In this high energy range, the potential energy curve in Fig. 1(a) is obviously not sufficient for explaining residence probabilities. In this report, we will present the mechanism of the switching of structural preference observed in Fig. 1(b) in terms of the effect of a dynamical and geometrical force that often counteracts with the potential force.

## 2.2 Coarse dynamics of gyration radii

Here, we coarsely characterize the structural transition dynamics of the  $M_6$  cluster using the three gyration radii, our collective variables. For generality, we consider an  $n$ -atom molecule whose constituent atoms have masses  $m_i$  ( $i = 1, \dots, n$ ). After eliminating the overall translational degrees of freedom of the molecule via the mass-weighted Jacobi vectors,

$$\rho_{si} = \sqrt{\frac{m_{i+1} \sum_{k=1}^i m_k}{\sum_{k=1}^{i+1} m_k}} \left( \frac{\sum_{k=1}^i m_k \mathbf{r}_{sk}}{\sum_{k=1}^i m_k} - \mathbf{r}_{s(i+1)} \right) \quad (i = 1, \dots, n-1), \quad (2)$$

the singular-value decomposition theorem [44] can be applied to decompose the  $3 \times (n-1)$ -dimensional matrix  $W_s \equiv (\rho_{s1} \dots \rho_{s(n-1)})$  into the product of the three matrices

$$W_s = RNU^T, \quad (3)$$

where  $R = (\mathbf{e}_1 \mathbf{e}_2 \mathbf{e}_3)$ , and

$$N = \left( \begin{array}{ccc|ccc} a_1 & 0 & 0 & 0 & \dots & 0 \\ 0 & a_2 & 0 & 0 & \dots & 0 \\ 0 & 0 & a_3 & 0 & \dots & 0 \end{array} \right) \equiv \left( \begin{array}{c|c} A & O \end{array} \right), \quad (4)$$

$$U = (\mathbf{u}_1 \mathbf{u}_2 \mathbf{u}_3 | \mathbf{u}_4 \dots \mathbf{u}_{n-1}) \equiv (P|Q). \quad (5)$$

The symbol  $T$  on the matrix  $U$  in Eq. (3) indicates the matrix transpose. The matrix  $R$  is a  $3 \times 3$  orthogonal matrix ( $SO(3)$ ), whose column vectors,  $\mathbf{e}_1, \mathbf{e}_2, \mathbf{e}_3$ , are orthogonal and normalized. The matrix  $N$  is a  $3 \times (n-1)$  diagonal matrix, which is split up into the left  $3 \times 3$  diagonal matrix  $A$  and the right  $3 \times (n-4)$  zero matrix  $O$  for later use. The diagonal elements (singular values),  $a_1, a_2, a_3$ , are the gyration radii, which are the key quantities of this study. Although there are many alternative definitions for the Jacobi vectors, gyration radii are independent of the choice of Jacobi vectors. They are non-negative and ordered according to  $a_1 \geq a_2 \geq a_3 \geq 0$ . The matrix  $U$  is an  $(n-1) \times (n-1)$  orthogonal matrix ( $SO(n-1)$ ), whose column vectors,  $\mathbf{u}_1, \dots, \mathbf{u}_{n-1}$ , are orthogonal and normalized.

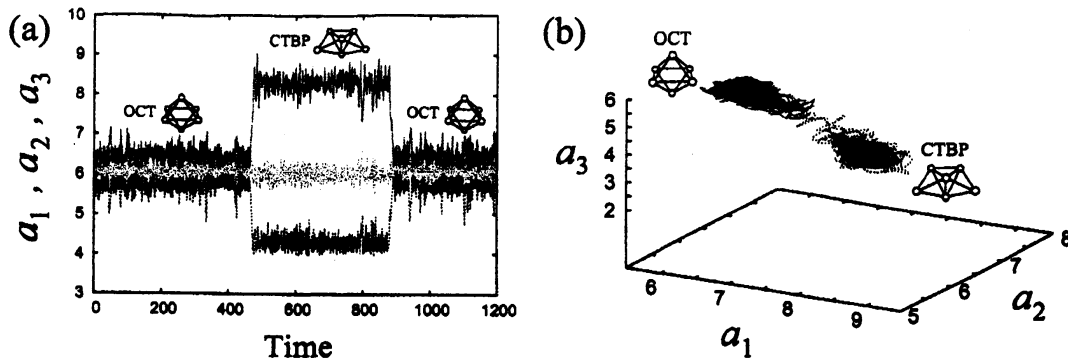


Figure 2: (a) Typical time evolution of the three gyration radii  $a_1$ ,  $a_2$ , and  $a_3$  ( $a_1 \geq a_2 \geq a_3$ ) of the  $M_6$  cluster at total energy  $E = -11.0\epsilon$ . The cluster quenches to the OCT isomer from  $t = 0$  to  $t = 468$  and from  $t = 884$  to  $t = 1200$ , while the cluster is quenched to the CTBP isomer from  $t = 468$  to  $t = 884$ . (b) The same trajectory as in (a) projected onto the three-dimensional space of gyration radii. The two trapping regions correspond to the two isomers, OCT (solid line) and CTBP (dashed line).

The matrix  $U$  is split up into the left  $(n-1) \times 3$  matrix  $P$  and the right  $(n-1) \times (n-4)$  matrix  $Q$  for later convenience.

The physical meaning of the decomposition Eq. (3) is as follows. It is shown that the matrix  $R$  coincides with the principal axis frame, which specifies the instantaneous orientation of the system, while  $N$  and  $U$  determine the internal structure (size and symmetry) of the system. Gyration radii,  $a_1, a_2, a_3$ , are the measure of the mass-weighted length of the system along the respective principal axes. They essentially characterize the *mass distribution*, and are related to the principal moments of inertia,  $M_1, M_2$ , and  $M_3$  ( $M_3 \geq M_2 \geq M_1 \geq 0$ ), by  $M_1 = a_2^2 + a_3^2$ ,  $M_2 = a_3^2 + a_1^2$ ,  $M_3 = a_1^2 + a_2^2$ . The values of the gyration radii of the  $M_6$  cluster at the potential minimum of the OCT isomer are  $(a_1, a_2, a_3) = (5.97, 5.97, 5.97)$ , while those of the CTBP isomer are  $(a_1, a_2, a_3) = (8.19, 5.89, 4.27)$ . The coincidence of the three gyration radii at the OCT structure indicates that it has isotropic mass distribution (spherical top). The CTBP structure has an asymmetric mass distribution.

Fig. 2(a) shows a typical time evolution of the three gyration radii of the  $M_6$  cluster at total energy  $E = -11.0\epsilon$ . In the time period of Fig. 2(a), the system first transited from the OCT isomer to the CTBP isomer. After a while it returned back to the OCT isomer. The isomerization reaction is clearly marked by the change of the three gyration radii. In each isomer, the three gyration radii take values close to those at the corresponding potential minimum. Fig. 2(b) shows the same trajectory as in Fig. 2(a) projected onto the three-dimensional space of gyration radii, which captures the changes of mass distribution of the system. In Fig. 2(b), the two regions corresponding to the OCT isomer and the CTBP isomer are distinguished. Both of the two regions are small when the total energy is low. As the total energy increases, the two regions become larger. The essential fact is that certain regions of the three-dimensional space of gyration radii and certain isomer wells of the cluster have good one-to-one correspondence. Therefore, the transition of the

trajectory in the three-dimensional space of gyration radii from one region to the other is indicative of a structural change of the full system. This is the most vital condition for the three gyration radii to be good collective variables. In general, gyration radii can characterize structural transitions of a molecule in this way as long as the system changes its mass distribution significantly through the transitions.

The number of total internal degrees of freedom of the  $M_6$  cluster is twelve. Therefore nine other internal degrees of freedom are "hidden" behind the dynamics in Fig. 2(b). If these hidden degrees of freedom can be regarded as "bath" modes, one can think of a closed dynamical system in terms of only the three gyration radii. If this is the case, one will be able to extract essential information about the structural transition of the full system from the low-dimensional dynamics of gyration radii. These are the main issues of this report in the following sections, where we will finally extract an effective barrier structure that separates the different isomer regions as in Fig. 2(b). These barrier structures will in turn explain the true dynamical stability of the respective isomers.

### 3 Equations of Motion for the Collective Variables

#### 3.1 Kinetic energy of an $n$ -atom molecule in the hyperspherical coordinates

The goal of this section is to derive classical equations of motion for the gyration radii, our collective variables, using the principal-axis hyperspherical coordinates. For this purpose, we first present the general expression for the total kinetic energy of an  $n$ -atom molecule, such as Eq. (27) and Eq. (29), in this subsection.

Let a matrix  $R \in \text{SO}(3)$  be a body (body-fixed) frame. Since the Jacobi vectors with respect to the body frame  $\rho_i$  ( $i = 1, \dots, n-1$ ) are related to the Jacobi vectors with respect to the space-fixed frame  $\rho_{si}$  ( $i = 1, \dots, n-1$ ) by  $\rho_{si} = R\rho_i$ , the time-derivative of  $\rho_{si}$  can be expressed as

$$\dot{\rho}_{si} = \dot{R}\rho_i + R\dot{\rho}_i. \quad (6)$$

Similarly, the total angular momentum with respect to the space-fixed frame  $L_s$  and that with respect to the body frame  $L$  are related by  $L_s = RL$ . Since

$$L_s = \sum_{i=1}^{n-1} \rho_{si} \times \dot{\rho}_{si}, \quad (7)$$

$L$  can be expressed as

$$L = R^T \sum_{i=1}^{n-1} \rho_{si} \times \dot{\rho}_{si} = M\Omega + \sum_{i=1}^{n-1} \rho_i \times \dot{\rho}_i. \quad (8)$$

The matrix  $M$  in Eq. (8) is the moment of inertia tensor with respect to the body frame, whose components are defined by

$$M_{\alpha\beta} = \sum_{i=1}^{n-1} [(\rho_i \cdot \rho_i) \delta_{\alpha\beta} - \rho_{i\alpha} \rho_{i\beta}], \quad (9)$$

where  $\alpha$  and  $\beta$  ( $\alpha, \beta = 1, 2, 3$ ) represent the axes of the body frame and  $\delta_{\alpha\beta}$  is the Kronecker delta. The vector  $\Omega \equiv (\Omega_1, \Omega_2, \Omega_3)^T$  in Eq. (8) is the angular velocity with respect to the body frame whose components are defined through the anti-symmetric matrix,

$$R^T \dot{R} \equiv \begin{pmatrix} 0 & -\Omega_3 & \Omega_2 \\ \Omega_3 & 0 & -\Omega_1 \\ -\Omega_2 & \Omega_1 & 0 \end{pmatrix}. \quad (10)$$

The kinetic energy of the system in a space fixed frame is given by

$$K = \frac{1}{2} \sum_{i=1}^n m_i (\dot{\mathbf{r}}_{si} \cdot \dot{\mathbf{r}}_{si}) = \frac{1}{2} \sum_{i=1}^{n-1} \dot{\boldsymbol{\rho}}_{si} \cdot \dot{\boldsymbol{\rho}}_{si}. \quad (11)$$

After applying Eq. (6) to Eq. (11), it can be expressed in terms of the body-frame quantities as

$$K = \frac{1}{2} \Omega^T M \Omega + \Omega^T \sum_{i=1}^{n-1} \boldsymbol{\rho}_i \times \dot{\boldsymbol{\rho}}_i + \frac{1}{2} \sum_{i=1}^{n-1} \dot{\boldsymbol{\rho}}_i \cdot \dot{\boldsymbol{\rho}}_i. \quad (12)$$

Now we reformulate the kinetic energy of Eq. (12) in terms of the principal-axis hyperspherical coordinates. In what follows, we identify the body frame  $R$  in the above argument with the principal-axis frame  $R$  introduced in Eq. (3). Correspondingly, the angular velocity vector  $\Omega$ , the moment of inertia tensor  $M$ , and the Jacobi vectors  $\{\boldsymbol{\rho}_i\}$  in Eq. (12) are all regarded as the ones with respect to the principal-axis frame.

The second term of Eq. (12) can be reformulated as follows. Based on Eq. (3), the Jacobi vectors  $\{\boldsymbol{\rho}_i\}$  with respect to the principal-axis frame are expressed collectively in a matrix form as

$$(\boldsymbol{\rho}_1 \cdots \boldsymbol{\rho}_{n-1}) = N U^T \equiv W. \quad (13)$$

where the  $3 \times (n-1)$  matrix  $W$  is a body-frame counterpart of  $W_s$  of Eq. (3). By using  $W$ , the components of  $\sum_{i=1}^{n-1} \boldsymbol{\rho}_i \times \dot{\boldsymbol{\rho}}_i \equiv (\xi_1, \xi_2, \xi_3)^T$  are given by

$$\begin{pmatrix} 0 & -\xi_3 & \xi_2 \\ \xi_3 & 0 & -\xi_1 \\ -\xi_2 & \xi_1 & 0 \end{pmatrix} = \dot{W} W^T - W \dot{W}^T = -2A P^T \dot{P} A, \quad (14)$$

where  $A$  and  $P$  are the sub-matrices defined in Eq. (4) and in Eq. (5). After introducing quasivelocity components

$$\dot{\mathbf{u}}_i \cdot \mathbf{u}_j = -\mathbf{u}_i \cdot \dot{\mathbf{u}}_j \equiv \omega_{ij} \quad (i, j = 1, 2, 3, i \neq j), \quad (15)$$

the anti-symmetric matrix  $P^T \dot{P}$  can be expressed as

$$P^T \dot{P} = \begin{pmatrix} 0 & -\omega_{12} & \omega_{31} \\ \omega_{12} & 0 & -\omega_{23} \\ -\omega_{31} & \omega_{23} & 0 \end{pmatrix}. \quad (16)$$

By substituting Eq. (16) into Eq. (14) and comparing the leftmost part with the rightmost part of Eq. (14), we obtain

$$\xi_1 = -2a_2 a_3 \omega_{23}, \quad \xi_2 = -2a_3 a_1 \omega_{31}, \quad \xi_3 = -2a_1 a_2 \omega_{12}. \quad (17)$$

These formulas allow us to express the second term on the right hand side of Eq. (12) finally as

$$\Omega^T \sum_{i=1}^{n-1} \rho_i \times \dot{\rho}_i = -2a_2a_3\Omega_1\omega_{23} - 2a_3a_1\Omega_2\omega_{31} - 2a_1a_2\Omega_3\omega_{12} \quad (18)$$

$$= \Omega^T \mathbf{B} \omega, \quad (19)$$

where the following two matrices are introduced for notational compactness:

$$\mathbf{B} = \begin{pmatrix} -2a_2a_3 & 0 & 0 \\ 0 & -2a_3a_1 & 0 \\ 0 & 0 & -2a_1a_2 \end{pmatrix}, \quad \omega = \begin{pmatrix} \omega_{23} \\ \omega_{31} \\ \omega_{12} \end{pmatrix}. \quad (20)$$

Similarly, the third term in the right hand side of Eq. (12) can also be reformulated using the matrix  $\mathbf{W}$  of Eq. (13) as

$$\frac{1}{2} \sum_{i=1}^{n-1} \dot{\rho}_i \cdot \dot{\rho}_i = \frac{1}{2} \text{Tr}(\dot{\mathbf{W}}\dot{\mathbf{W}}^T) \quad (21)$$

$$= \frac{1}{2} \text{Tr}(\dot{\mathbf{A}}\dot{\mathbf{A}}^T) + \frac{1}{2} \text{Tr}(\mathbf{A}\dot{\mathbf{P}}^T \mathbf{P}\mathbf{P}^T \dot{\mathbf{P}}\mathbf{A}) + \frac{1}{2} \text{Tr}(\mathbf{A}\dot{\mathbf{P}}^T \mathbf{Q}\mathbf{Q}^T \dot{\mathbf{P}}\mathbf{A}), \quad (22)$$

where  $\text{Tr}(\cdot)$  represents the trace of a matrix and where  $\mathbf{A}$ ,  $\mathbf{P}$ , and  $\mathbf{Q}$  are the matrices defined in Eq. (4) and in Eq. (5). After introducing the quasivelocity components,

$$\dot{\mathbf{u}}_i \cdot \mathbf{u}_j = -\mathbf{u}_i \cdot \dot{\mathbf{u}}_j \equiv \gamma_{ij} \quad (i = 1, 2, 3, \quad j = 4, \dots, n-1), \quad (23)$$

the  $(n-4) \times 3$  matrix  $\mathbf{Q}^T \dot{\mathbf{P}}$  in Eq. (22) can be expressed as

$$\mathbf{Q}^T \dot{\mathbf{P}} = \begin{pmatrix} \gamma_{14} & \gamma_{24} & \gamma_{34} \\ \vdots & \vdots & \vdots \\ \gamma_{1(n-1)} & \gamma_{2(n-1)} & \gamma_{3(n-1)} \end{pmatrix} \equiv \begin{pmatrix} \gamma_1 & \gamma_2 & \gamma_3 \end{pmatrix}, \quad (24)$$

where we have introduced the  $(n-4)$ -dimensional column vectors  $\gamma_i$  ( $i = 1, 2, 3$ ). By applying Eq. (16) and Eq. (24) to Eq. (22), we obtain the final expression for the third term of Eq. (12) as

$$\begin{aligned} \frac{1}{2} \sum_{i=1}^{n-1} \dot{\rho}_i \cdot \dot{\rho}_i &= \frac{1}{2} (\dot{a}_1^2 + \dot{a}_2^2 + \dot{a}_3^2) + \frac{1}{2} (M_1\omega_{23}^2 + M_2\omega_{31}^2 + M_3\omega_{12}^2) \\ &\quad + \frac{1}{2} a_1^2 \sum_{k=4}^{n-1} \gamma_{1k}^2 + \frac{1}{2} a_2^2 \sum_{k=4}^{n-1} \gamma_{2k}^2 + \frac{1}{2} a_3^2 \sum_{k=4}^{n-1} \gamma_{3k}^2, \end{aligned} \quad (25)$$

$$= \frac{1}{2} \dot{\mathbf{a}} \cdot \dot{\mathbf{a}} + \frac{1}{2} \omega^T \mathbf{M} \omega + \frac{1}{2} \sum_{i=1}^3 \gamma_i^T a_i^2 \gamma_i, \quad (26)$$

where  $\mathbf{a} \equiv (a_1, a_2, a_3)^T$ , and  $\mathbf{M}$  is the moment of inertia tensor with respect to the principal-axis frame.

Substituting Eq. (19) and Eq. (26) into Eq. (12), we obtain the desired general expression for the total kinetic energy of an  $n$ -atom molecule as

$$K = \frac{1}{2}\Omega^T M \Omega + \Omega^T B \omega + \frac{1}{2}\dot{\mathbf{a}} \cdot \dot{\mathbf{a}} + \frac{1}{2}\omega^T M \omega + \frac{1}{2} \sum_{i=1}^3 \gamma_i^T a_i^2 \gamma_i, \quad (27)$$

which is essentially the same as the one given by Eckart [20] and by Chapuisat *et al.* [21]. Introduction of the quasi-velocities,  $\omega$  and  $\gamma_i$ , has been crucial in making this a compact expression; in it, the  $(3n - 6)$  internal degrees of freedom are represented by the three gyration radii and the  $(3n - 9)$  quasivelocity components. These quasivelocities are essentially the "angular velocities" of kinematic (or democratic) rotations, which are continuous shape changes associated with the permutations (relabellings) among the constituent atoms [23–28]. They should be distinguished from the angular velocity of the principal-axis frame  $\Omega$ .

### 3.2 Equations of motion for gyration radii under the conditions of vanishing total angular momentum

We next investigate the equations of motion for the three gyration radii,  $a_1$ ,  $a_2$ , and  $a_3$ , under the conditions of zero total angular momentum. Since the total angular momentum with respect to the body frame is given by

$$\mathbf{L} = \mathbf{M}\Omega + \mathbf{B}\omega, \quad (28)$$

after using Eq. (8) and Eq. (19), the total kinetic energy can be expressed as follows after applying Eq. (28) to Eq. (27),

$$K = \frac{1}{2}\mathbf{L}^T \mathbf{M}^{-1} \mathbf{L} + \frac{1}{2}\dot{\mathbf{a}} \cdot \dot{\mathbf{a}} + \frac{1}{2}\omega^T \tilde{\mathbf{M}} \omega + \frac{1}{2} \sum_{i=1}^3 \gamma_i^T a_i^2 \gamma_i, \quad (29)$$

where we have introduced a diagonal matrix,

$$\tilde{\mathbf{M}} \equiv \mathbf{M} - \mathbf{B}\mathbf{M}^{-1}\mathbf{B} = \begin{pmatrix} \frac{(a_2^2 - a_3^2)^2}{(a_2^2 + a_3^2)} & 0 & 0 \\ 0 & \frac{(a_3^2 - a_1^2)^2}{(a_3^2 + a_1^2)} & 0 \\ 0 & 0 & \frac{(a_1^2 - a_2^2)^2}{(a_1^2 + a_2^2)} \end{pmatrix}. \quad (30)$$

The expression of Eq. (29) is important from the gauge-theoretical point of view [19]: Each term of Eq. (29) is independent of the choice of body frame, while the kinetic energy expression of Eq. (27) is specific to the principal-axis choice of body frame. By applying the zero angular momentum condition,  $\mathbf{L} = \mathbf{0}$ , to Eq. (29), we obtain the purely internal

kinetic energy,

$$\begin{aligned}
K &= \frac{1}{2} \dot{\mathbf{a}} \cdot \dot{\mathbf{a}} + \frac{1}{2} \boldsymbol{\omega}^T \tilde{\mathbf{M}} \boldsymbol{\omega} + \frac{1}{2} \sum_{i=1}^3 \gamma_i^T a_i^2 \gamma_i, \quad (31) \\
&= \frac{1}{2} (\dot{a}_1^2 + \dot{a}_2^2 + \dot{a}_3^2) + \frac{(a_1^2 - a_2^2)^2}{2(a_1^2 + a_2^2)} \omega_{12}^2 + \frac{(a_2^2 - a_3^2)^2}{2(a_2^2 + a_3^2)} \omega_{23}^2 + \frac{(a_3^2 - a_1^2)^2}{2(a_3^2 + a_1^2)} \omega_{31}^2 \\
&\quad + \frac{1}{2} a_1^2 \sum_{k=4}^{n-1} \gamma_{1k}^2 + \frac{1}{2} a_2^2 \sum_{k=4}^{n-1} \gamma_{2k}^2 + \frac{1}{2} a_3^2 \sum_{k=4}^{n-1} \gamma_{3k}^2. \quad (32)
\end{aligned}$$

At this point, it is important to note that the mass metric components for  $\dot{a}_1^2$ ,  $\dot{a}_2^2$ , and  $\dot{a}_3^2$  are all equal to unity. This means that the three-dimensional space of gyration radii such as Fig. 2(b) is *Euclidean* even though the  $(3n - 6)$ -dimensional full internal space is non-Euclidean. This will be of great advantage in the following discussions in reducing the full dynamics of a molecule to the three-dimensional space of gyration radii.

By using the internal kinetic energy Eq. (32), the Lagrangian for the  $n$ -atom molecule with vanishing total angular momentum is given by  $\mathcal{L} = K - V$ . Recall that for our study of isolated molecules the potential energy  $V$  is a function only of the internal degrees of freedom. The Euler-Lagrange equations for the gyration radii can be written as

$$\ddot{a}_1 = \frac{a_1 (a_1^2 + 3a_2^2) (a_1^2 - a_2^2)}{(a_1^2 + a_2^2)^2} \omega_{12}^2 + \frac{a_1 (a_1^2 + 3a_3^2) (a_1^2 - a_3^2)}{(a_1^2 + a_3^2)^2} \omega_{13}^2 + a_1 \sum_{k=4}^{n-1} \gamma_{1k}^2 - \frac{\partial V}{\partial a_1}, \quad (33)$$

$$\ddot{a}_2 = \frac{a_2 (a_2^2 + 3a_1^2) (a_2^2 - a_1^2)}{(a_2^2 + a_1^2)^2} \omega_{21}^2 + \frac{a_2 (a_2^2 + 3a_3^2) (a_2^2 - a_3^2)}{(a_2^2 + a_3^2)^2} \omega_{23}^2 + a_2 \sum_{k=4}^{n-1} \gamma_{2k}^2 - \frac{\partial V}{\partial a_2}, \quad (34)$$

$$\ddot{a}_3 = \frac{a_3 (a_3^2 + 3a_2^2) (a_3^2 - a_2^2)}{(a_3^2 + a_2^2)^2} \omega_{32}^2 + \frac{a_3 (a_3^2 + 3a_1^2) (a_3^2 - a_1^2)}{(a_3^2 + a_1^2)^2} \omega_{31}^2 + a_3 \sum_{k=4}^{n-1} \gamma_{3k}^2 - \frac{\partial V}{\partial a_3}. \quad (35)$$

The left hand sides of these equations are the components of acceleration in the three-dimensional space of gyration radii. The right hand sides are physically the forces in this space. While the fourth terms on the right hand sides of Eqs. (33)-(35) represent the force that originates from the potential energy function, the first three terms on the right hand sides of these equations represent a *dynamic (kinematic) force* that originates from the dynamical coupling of gyration radii with the kinematic-rotation modes. All of these dynamic force terms are quadratic in the quasivelocity components,  $\omega_{ij}$  and  $\gamma_{ik}$ . Therefore, these terms essentially represent the *internal centrifugal force* arising from the kinematic rotations. It has been shown that the internal centrifugal terms proportional to  $\omega_{ij}^2$  arise in the three- and four-atom dynamics [32]. But the internal centrifugal force terms proportional to  $\gamma_{ik}^2$  are intrinsic to systems with more than four-atom systems in the three-dimensional physical space. As the number of atoms increases, the number of the terms proportional to  $\gamma_{ik}^2$  increases.

While the force arising from the potential function is dependent on the system, the internal centrifugal force terms in Eqs. (33)-(35) are common to the dynamics of general  $n$ -atom molecules. Therefore it is quite interesting to explore the essential properties

of this kinematic force. The internal centrifugal force terms proportional to  $\omega_{ij}^2$  have an effect of breaking the symmetry of mass distribution of the  $n$ -atom molecule. This property can be understood by noting the sign of the corresponding terms in Eqs. (33)-(35): Since  $a_1 \geq a_2 \geq a_3 \geq 0$  holds by definition, the first and the second terms in Eq. (33) are always positive or zero. This means that these terms have a persistent effect of enlarging the largest gyration radius  $a_1$ . On the other hand, by similar arguments, the first and the second terms in Eq. (35) are always negative or zero. These terms will therefore persistently diminish the smallest gyration radius  $a_3$ . Finally, the first term of Eq. (34) is negative or zero and the second term of Eq. (34) is positive or zero. Therefore, the force can act both positively and negatively for  $a_2$ . Since the gyration radii are the measure of the mass-weighted size of the system along the principal axes, these properties of the internal centrifugal force indicate that *a molecule is always forced to elongate in the most massive direction and to collapse in the least massive direction*. The terms proportional to  $\gamma_{ij}^2$  in Eqs. (33)-(35) are always positive. Therefore, these have an effect of *inflating* the molecule in all three principal axis directions. It is expected that the inflating effect becomes greater as the number of atoms increase since the number of the terms proportional to  $\gamma_{ij}^2$  increases.

The internal centrifugal force discussed above have similarities to those of the normal centrifugal force. However the origins of the internal centrifugal force and the normal centrifugal force are different. The normal centrifugal force is associated with the non-zero total angular momentum, and is thereby absent in the system with zero total angular momentum. On the other hand, the internal centrifugal force of this study is associated with the kinematic rotations and can arise even in the dynamics with zero angular momentum. That is, the internal centrifugal force is essentially a dynamical force induced by molecular vibrations themselves. In the next section, we scrutinize the competition between this kind of dynamical force and the ordinary potential force.

## 4 Dynamics of Collective Variables: Competition between Dynamic Force and Potential Force

### 4.1 Distinction between collective variables and “bath” modes

In this section, we scrutinize the low dimensional dynamics of gyration radii on the basis of the equations of motion presented in the previous section and numerical experiments. Competition between the internal centrifugal force and the potential force is highlighted.

We first clarify the distinction between collective variables and “bath” modes. Fig. 3 shows the typical time evolution of (a) the gyration radii  $a_1$ ,  $a_2$ , and  $a_3$ , (b) the squares of the quasivelocities  $\omega_{ij}^2$ , (c)  $\gamma_i^2 \equiv \gamma_{i4}^2 + \gamma_{i5}^2$  ( $i = 1, 2, 3$ ) at total energy  $E = -10.0\epsilon$ . During the time interval of Fig. 3, the cluster had undergone isomerization from the OCT isomer to the CTBP isomer once. In Fig. 3, we see that the three gyration radii,  $a_1$ ,  $a_2$ , and  $a_3$ , change slowly and smoothly, in contrast to the internal quasivelocidity components,  $\omega_{ij}^2$  and  $\gamma_i^2$ , which oscillate rapidly and sharply. This result supports the ansatz that the gyration radii can be considered as slow variables while other internal modes behave like “bath” modes. The rapid oscillations of the quasivelocities induce the rapid oscillations

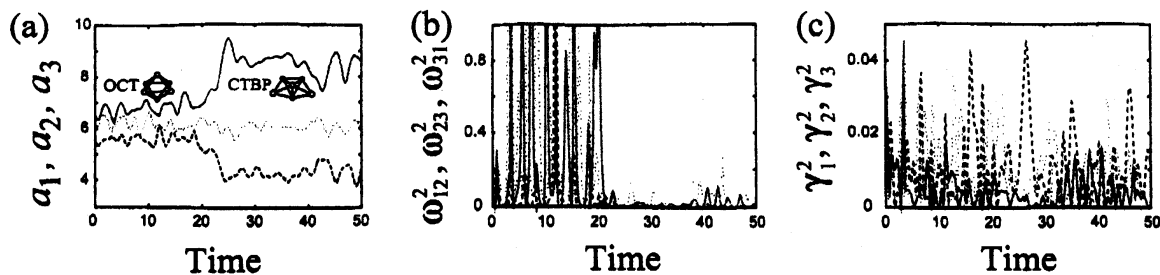


Figure 3: Typical time evolution of (a) the three gyration radii  $a_1, a_2,$  and  $a_3$ , (b) the squares of the quasivelocities,  $\omega_{12}^2, \omega_{23}^2, \omega_{31}^2$ , (c)  $\gamma_1^2, \gamma_2^2, \gamma_3^2$  at total energy  $E = -10.0\epsilon$ . The system quenches to OCT from  $t = 0$  to  $t = 21.5$ , and to CTBP from  $t = 21.5$  to  $t = 50$ .

of the internal centrifugal force in the dynamics of gyration radii. This result justifies our strategy of averaging the rapid oscillations of the forces in Eqs. (33)-(35) to deduce effective force fields that the gyration radii “feel” as will be shown in the next subsection.

We next present another dynamical evidence that gyration radii play a predominant role over other hyperangular variables in the large-amplitude motions of the cluster. Open squares in Fig. 4(a) represent average kinetic energies in the 12 internal modes of the  $M_6$  cluster when the cluster is in the OCT isomer. Here, each term in Eq. (32) represents the kinetic energy in each mode. Open circles represent the similar average kinetic energy distribution when the system is in the CTBP isomer. The total internal energy of the cluster is  $E = -10.0\epsilon$ . It is evident that the kinetic energy is partitioned equally among the 12 internal modes in both the OCT and CTBP isomers. That is, kinetic energy is equipartitioned among all the internal modes when the cluster is in each of the two isomer. On the other hand, Fig. 4(b) shows the kinetic energy distribution among internal modes averaged *over reactive trajectories*. As opposed to Fig. 4(a), we see that kinetic energy is not equipartitioned, but the  $a_1$  and  $a_3$  modes have markedly (about 1.5 ~ 2 times) more kinetic energy than other internal modes. Note that the kinetic energy distribution is almost the same for the reaction from OCT to CTBP and the reverse reaction from CTBP to OCT. This is due to time reversal symmetry of the system. The result of Fig. 4(b) indicates that the two gyration radii  $a_1$  and  $a_3$  must acquire more kinetic energy than other internal degrees of freedom for both the forward and backward reaction. This clearly shows that the gyration radii play a predominant role over other internal variables in the large-amplitude motion.

## 4.2 Characterization of the potential force and the internal centrifugal force via averaging

Based on the results in the previous subsection, we regard the three gyration radii as predominant collective variables (reaction coordinates), and all other hyperangular modes are regarded as “bath” modes in this study. For the understanding of the mechanism of structural transition of the cluster, the next important step is to characterize the competition between the internal centrifugal force and the potential force in the dynamics

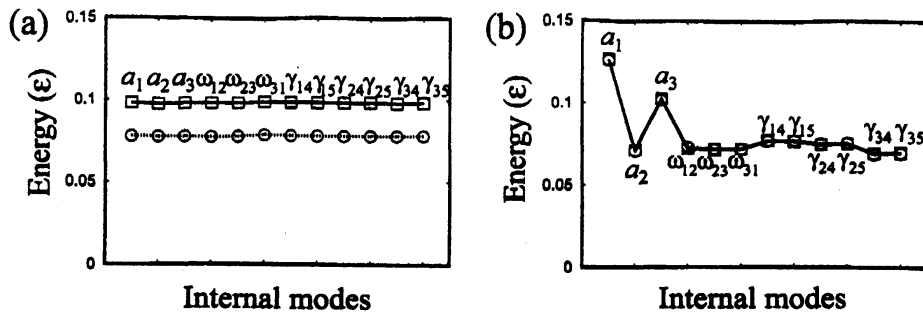


Figure 4: (a) Open squares represent the average kinetic energies distributed into the 12 internal modes of the  $M_3$  cluster when the system is in the OCT isomer. Open circles represent the average kinetic energies distributed among the 12 internal modes when the system is in the CTBP conformation. (b) Average kinetic energies partitioned by the 12 internal modes over reactive trajectories. Open squares correspond to the reaction from OCT to CTBP, and open circles correspond to the reaction from CTBP to OCT.

of gyration radii. We here deduce an averaged field of the internal centrifugal force and that of the potential force numerically along a one-dimensional reaction path introduced in the space of gyration radii. The reaction path is determined by directly averaging the trajectories in the space of gyration radii as in Fig. 2(b) in the following way: First, the trajectories are averaged in terms of the  $a_2$  and  $a_3$  components with  $a_1$  fixed to different values. We then obtain representative (averaged) points for respective  $a_1$  values. These representative points are connected successively to obtain a single path.

The internal centrifugal force and the potential force can now be characterized along the averaged reaction path. Since these two forces oscillate rapidly as compared with the time scale of variation of gyration radii as a result of the rapid oscillations of the hyperangular variables (see Fig. 3 and Ref. [35]), it is reasonable to average out the time-dependence of these forces in the dynamics of gyration radii. In Fig. 5, shown with arrows are (a) the averaged field of the internal centrifugal force (the sum of the first three terms on the right hand sides of Eqs. (33)-(35)), and (b) that of the potential force (the fourth terms on the right hand sides of Eqs. (33)-(35)) along the reaction path at total energy  $E = -10.0\epsilon$ . In the figures, the averaged reaction path is shown by the thin broken curve. The averaged field of internal centrifugal force is roughly directed from the region of the OCT isomer to that of the CTBP isomer. Furthermore, the internal centrifugal force is stronger in the OCT region than in the CTBP region. This indicates that the internal centrifugal force strongly “pushes” the system from the OCT region to the CTBP region. On the other hand, the averaged potential force field along the reaction path in Fig. 5(b) exhibits a change in direction, roughly pointing, locally, to both points corresponding to the potential minima of the OCT and the CTBP isomer. In other words, the potential force is directed towards the minima of the potential wells in the reduced space of gyration radii as is naturally expected. Thus, the averaged potential force works to keep the internal mass distribution of the cluster close to that of each potential minimum structure, while the averaged internal centrifugal force has a persistent tendency to bring the system mass

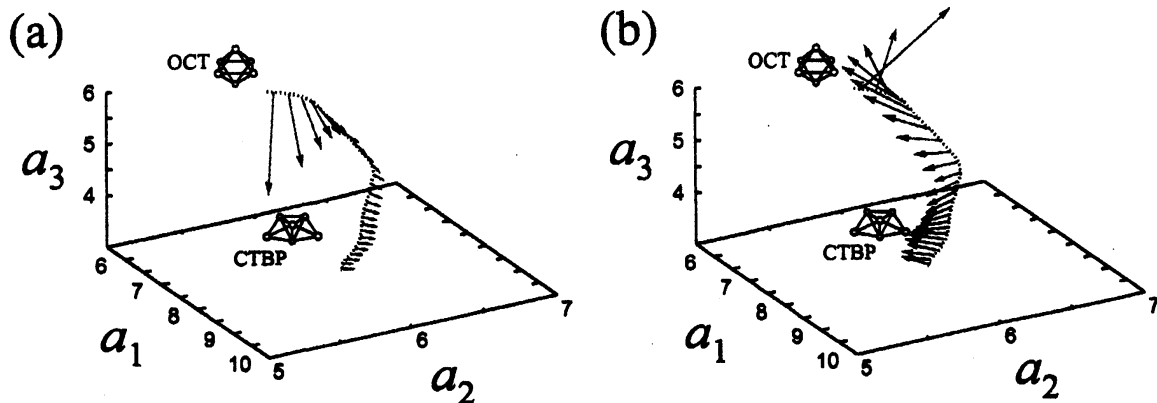


Figure 5: Averaged field of the internal centrifugal force (Panel (a)) and that of the potential force (Panel (b)) along the reaction path at  $E = -10.0\epsilon$ . The thin broken lines in the two figures constitute the averaged reaction path at  $E = -10.0\epsilon$ . The arrows represent the directionality and the magnitude of respective forces at each point along the reaction path. The thick solid curve is the projection of the steepest descent path onto the space for comparison.

distribution from that of the OCT isomer to that of the CTBP isomer.

### 4.3 Characterization of a dynamic barrier for reaction

The results in Fig. 5(a) indicate that the internal centrifugal force can be a *dynamic driving force* for the reaction from OCT to CTBP, while it can be a *dynamic barrier* for the reaction from CTBP to OCT. This, in turn, indicates that an extra amount of “work” may be needed in order for the vibrating cluster to change its gyration radii in addition to the work necessary to overcome the potential forces. Here, we quantify these two works by considering the line integrals of the two forces along the reaction path. This procedure gives a possible rationalization for the energy-dependent switching of the favored mass distribution of the  $M_6$  cluster presented in Fig. 1(b).

In Fig. 6, the upper three panels show the probability distributions along the reaction paths for different energies, (a)  $E = -11.2\epsilon$ , (b)  $E = -10.0\epsilon$ , and (c)  $E = -8.5\epsilon$ . The horizontal axis of each of these figures is the arc-length along each reaction path in the space of gyration radii, which serves as the reaction coordinate. The left part (the short arc-length part) of each figure corresponds to the region of the OCT isomer, while the right part corresponds to the region of the CTBP isomer. Since the reaction path becomes longer as the total energy increases, the width of these panels increases from (a) to (c). In each panel, two peaks are observed in the probability distribution, the left one of which corresponds to the OCT isomer while the right one corresponds to the CTBP isomer. At low total energy (Fig. 6(a)), the left peak is higher than the right peak. This indicates that the system prefers to be in the mass distribution of the OCT isomer than that of CTBP. On the other hand, as the total energy increases (Fig. 6(b) and (c)), the left peak is lowered and the right peak becomes higher. In other words, the preferable mass distribution of the cluster switches from that of the OCT isomer to that of the CTBP

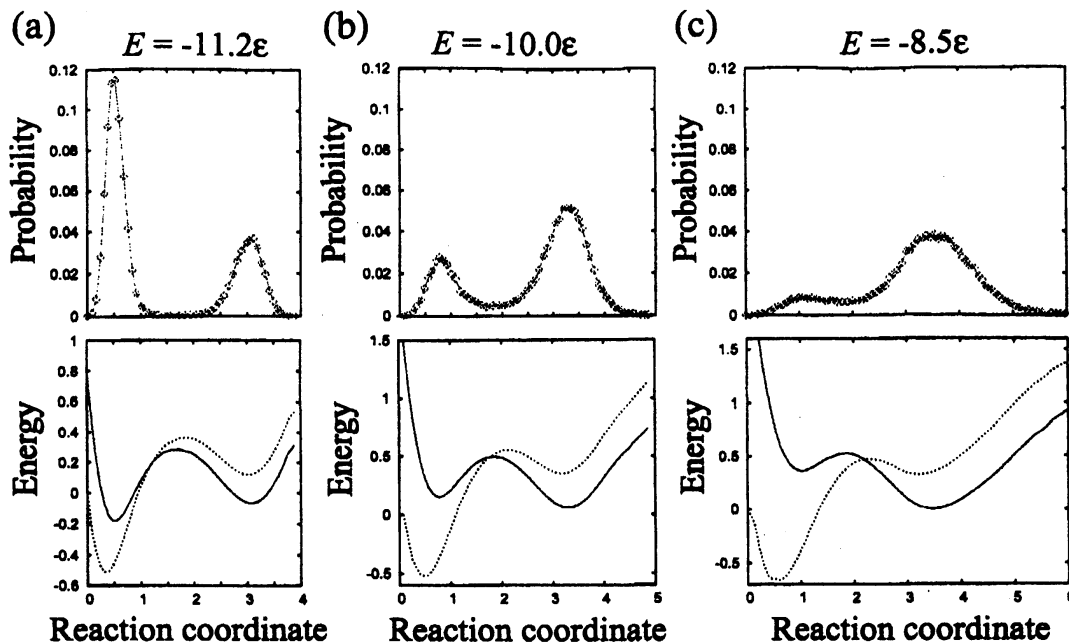


Figure 6: The upper three panels represent the probability distribution along the reaction coordinates introduced at total energy (a)  $E = -11.2\epsilon$ , (b)  $E = -10.0\epsilon$ , and (c)  $E = -8.5\epsilon$ . The lower three panels represent the corresponding reconstructed potential energy  $V_{\text{pot}}$  (dotted line), and the superposed potential  $V_{\text{pot+cent}}$  (solid line) along the reaction coordinates.

isomer. In this way, the switching of the structural preference observed in Fig. 1(b) is characterized in terms of the reaction paths. This kind of switching in the probability distribution is analogous to first-order-like phase transitions observed in clusters [39–41] and polymers [42, 43].

Now, the mechanism of the switching to the favored isomer can be rationalized in terms of the “work” necessary to bring the system against the averaged force fields obtained in Figs. 5(a) and (b). The line integral of the negative of the averaged potential force field ( $\langle f_{\text{pot},1} \rangle, \langle f_{\text{pot},2} \rangle, \langle f_{\text{pot},3} \rangle$ ) along the reaction path gives a reconstructed potential energy curve  $V_{\text{pot}}$  as

$$V_{\text{pot}} = - \int_{\text{path}} \sum_{i=1}^3 \langle f_{\text{pot},i} \rangle da_i. \quad (36)$$

We carried out this line integral numerically starting at one of the end points of the reaction path, where the  $a_1$  is the smallest. Since the absolute value of the potential energy is arbitrary, we set  $V_{\text{pot}}$  to zero at the starting point of the line integral. The potential  $V_{\text{pot}}$  is essentially the reduced potential energy curve that the gyration radii feel along the reaction coordinate. In the lower three panels of Fig. 6,  $V_{\text{pot}}$  is shown for the three representative total energy values,  $E = -11.2\epsilon$ ,  $-10.0\epsilon$ , and  $-8.5\epsilon$ , with dotted curves. The essential topography of  $V_{\text{pot}}$  does not change significantly depending on the total energy. That is,  $V_{\text{pot}}$  always has two wells. The left well corresponds to the OCT

isomer while the right one corresponds to the CTBP isomer. The well for the OCT isomer is always much deeper than that for the CTBP isomer. The potential  $V_{\text{pot}}$  resembles the original potential energy curve along the steepest descent path shown in Fig. 1(a). The curve of  $V_{\text{pot}}$  is obviously not sufficient for explaining the energy-dependent change of the probability distribution along the reaction paths shown in the upper panels of Fig. 6.

We next superpose the effect of the internal centrifugal force over that of the potential curve  $V_{\text{pot}}$ . Similarly to Eq. (36), a superposed line integral of the averaged potential force and the averaged internal centrifugal force ( $\langle f_{\text{cent},1} \rangle, \langle f_{\text{cent},2} \rangle, \langle f_{\text{cent},3} \rangle$ ) is introduced as

$$V_{\text{pot+cent}} = - \int_{\text{path}} \sum_{i=1}^3 (\langle f_{\text{pot},i} \rangle + \langle f_{\text{cent},i} \rangle) da_i. \quad (37)$$

The solid curves in the lower three panels of Fig. 6 are the superposed energy  $V_{\text{pot+cent}}$ . Similarly to the curve of  $V_{\text{pot}}$ , this energy curve  $V_{\text{pot+cent}}$  shows two wells corresponding to the two isomers. However, the topography of  $V_{\text{pot+cent}}$  changes dramatically depending on the total energy of the system. At low total energy,  $E = -11.2\varepsilon$ , the left well of  $V_{\text{pot+cent}}$ , which corresponds to the OCT isomer, is deeper than the right well that corresponds to the CTBP isomer. As the total energy increases, the left well gets shallower while the right well gets deeper. This is because the effect of the internal centrifugal force becomes more significant as the total energy of the dynamics increases, while the potential curve  $V_{\text{pot}}$  does not change significantly. Note that the internal centrifugal force has the directionality to “push” the system from the OCT region to the CTBP region as confirmed in Fig. 5(a). In this way, the OCT isomer becomes less stable dynamically while the CTBP isomer becomes more preferred as total energy increases. This dramatic change of the superposed energy curve  $V_{\text{pot+cent}}$  explains the change of the probability distribution in the upper panels of Fig. 6 fairly well. To summarize, the predominance of the OCT isomer at low energy is mainly supported by the predominance of the potential force, while the predominance of the CTBP isomer at high energy is mainly supported by the predominance of the internal centrifugal force.

## 5 Summary and Outlook

By taking up the structural transition dynamics of a six-atom cluster as an illustrative example, we have presented a general methodology to elucidate the mechanism for large-amplitude collective motions of molecules with many degrees of freedom in terms of the reduced dynamics of the three molecular gyration radii. Based on the framework of geometric mechanics, we have first separated the three rotational degrees of freedom and the  $(3n - 6)$  internal degrees of freedom of an  $n$ -atom system. Then we have applied the principal-axis hyperspherical coordinates to further decompose the total  $(3n - 6)$  internal degrees of freedom into the three gyration radii and the  $(3n - 9)$  hyperangular modes. The three gyration radii are regarded as slow and collective variables, while the remaining hyperangular variables are regarded as “bath” modes. This classification of variables into collective and “bath” variables has been supported by the numerical observations on time scale separation and kinetic energy partitioning. The time scale separation has justified

our strategy to average out the hyperangular variables from the equations of motion for the three gyration radii, our collective variables.

We have scrutinized the averaged equations of motion for the gyration radii to reveal the mechanism of competition between a kinematic force and the potential force in the large-amplitude motions of the cluster. The kinematic force is identified as an internal centrifugal force that arises from the dynamical coupling of gyration radii with the hyperangular modes via the intrinsic non-Euclidean metric of the internal space. This internal centrifugal force has the remarkable effect of elongating and inflating the mass distribution of the system. These effects often counteract the effect of the potential force, which generally serves to keep the mass distribution of the system symmetric and compact. Via the competition between these two forces, the most preferable conformation of the system is determined.

While the potential function is specific to the system of interest, the kinetic energy expressions such as Eq. (29) and Eq. (32) are common to general  $n$ -atom molecules. Therefore the internal centrifugal force terms in Eqs. (33)-(35) also arise ubiquitously in the dynamics of general  $n$ -atom molecules. From this reason, the elongation and the inflation effects of the internal centrifugal force should be of general importance in a wide class of molecular reactions, where the system significantly changes its mass distribution. For example, because of the directionality of this force, its roles should be important in dissociation and recombination reactions.

It is an interesting next step to elucidate the phase space structure that mediates the low-dimensional dynamics of gyration radii. Recently, the dynamical systems approach has provided a mathematical basis for the study of non-statistical reaction processes of molecules [45-49]. Since the high-dimensional nature of phase space has often prevented from applying the dynamical systems approach to molecular reactions, our strategy to focus on the low-dimensional dynamics of gyration radii should be very useful. The phase space structure of the reduced dynamics of molecular gyration radii will be scrutinized in our future publications. We also plan to extend the present methodology to the systems in several different environments: Large-amplitude motions of molecules with non-zero total angular momentum are an interesting issue for the next step, in which the kinematic forces such as the (normal) centrifugal force and the Coriolis force also come into play in addition to the internal centrifugal force of this study. It is also an interesting issue to extend the present approach to the systems in thermal environments such as biomolecules. Since the internal centrifugal force has a general tendency to become strong in high energy (or temperature) range and has an effect of inflating and elongating the system, this force is naturally expected as a driving force for the unfolding of proteins.

Finally, an important consequence of the present study is that molecular vibrations themselves can induce a dynamical force such as the internal centrifugal force, which can be a critical driving force for large-amplitude motions of the system. It would be interesting to note that this kind of dynamic forces are quite analogous to the dynamic forces that stabilize the inverted pendulum whose suspension point is violently vibrated [50] as well as the particles in electromagnetic traps [51]. Obviously, the importance of this kind of dynamical effect has not been fully appreciated in the current reaction-rate theories. In the current standard reaction-rate theories, molecular reactions are usually regarded as an event in which a system surmounts a barrier of (Born-Oppenheimer) potential energy

along a certain reaction coordinate. However, the result of the present study and another recent one [52] suggest that dynamic forces, such as the internal centrifugal force, modify the original potential energy barrier significantly and induces another dynamical barrier for reactions. Thus, in order to improve the current reaction-rate theories, it would be very important to take into consideration not only the static potential energy barriers but also such dynamic barriers. This kind of dynamic barriers should definitely shed new light on the conventional picture of molecular reactions.

## Acknowledgments

This report is based on the joint work with Wang S. Koon (Caltech), Jerrold E. Marsden (Caltech), and Ioannis G. Kevrekidis (Princeton University). The author thanks for their very stimulating discussions and thoughtful suggestions in developing this research.

## References

- [1] R. Zwanzig, *Phys. Rev.* **124**, 983 (1961).
- [2] H. Mori, *Prog. Theor. Phys.* **33**, 423 (1965).
- [3] R. Zwanzig, *Nonequilibrium Statistical Mechanics* (Oxford University Press, New York, 2001).
- [4] A. Laio and M. Parrinello, *Proc. Natl. Acad. Sci.* **99** 12562 (2002).
- [5] R. Elber, A. Cárdenas, A. Ghosh, and H. A. Stern, *Adv. Chem. Phys.* **126**, 93 (2003).
- [6] G. Hummer and I. G. Kevrekidis, *J. Chem. Phys.* **118**, 10762 (2003).
- [7] D. I. Kopelevich, A. Z. Panagiotopoulos, and I. G. Kevrekidis, *J. Chem. Phys.* **122**, 044907 (2005); **122**, 044908 (2005).
- [8] W. H. Miller, N. C. Handy, and J. E. Adams, *J. Chem. Phys.* **72**, 99 (1980).
- [9] P. G. Bolhuis, D. Chandler, C. Dellago, and P. L. Geissler, *Annu. Rev. Phys. Chem.* **53**, 291 (2002).
- [10] W. E, W. Ren, and E. Vanden-Eijnden, *Chem. Phys. Lett.* **413**, 242 (2005).
- [11] J. E. Marsden, T. S. Ratiu, and J. Scheurle, *J. Math. Phys.* **41**, 3379 (2000).
- [12] J. E. Marsden and T. S. Ratiu, *Introduction to Mechanics and Symmetry* (Springer, New York, 1999).
- [13] M. Kummer, *Indiana Univ. Math. J.*, **30**, 281 (1981).
- [14] J. E. Marsden, R. Montgomery, and T. Ratiu, *Contemp. Math.* **28**, 101 (1984).

- [15] A. Guichardet, *Ann. Inst. H. Poincaré* **40**, 329 (1984).
- [16] T. Iwai, *Ann. Inst. H. Poincaré* **47**, 199 (1987).
- [17] T. Iwai, *J. Math. Phys.* **28**, 964 (1987).
- [18] A. Tachibana and T. Iwai, *Phys. Rev. A* **33**, 2262 (1986).
- [19] R. G. Littlejohn and M. Reinsch, *Rev. Mod. Phys.* **69**, 213 (1997).
- [20] C. Eckart, *Phys. Rev.* **46**, 383 (1934).
- [21] X. Chapuisat and A. Nauts, *Phys. Rev. A* **44**, 1328 (1991).
- [22] X. Chapuisat, *Phys. Rev. A* **45**, 4277 (1992).
- [23] A. Kuppermann, *Adv. Mol. Vib. Col. Dyn.* **2B**, 117 (1993).
- [24] A. Kuppermann, *J. Phys. Chem.* **100**, 2621 (1996).
- [25] A. Kuppermann, *J. Phys. Chem.* **101**, 6368 (1997).
- [26] R. G. Littlejohn and M. Reinsch, *Phys. Rev. A* **52**, 2035 (1995).
- [27] R. G. Littlejohn, K. A. Mitchell, V. A. Aquilanti, and S. Cavalli, *Phys. Rev. A* **58**, 3705 (1998).
- [28] R. G. Littlejohn, K. A. Mitchell, M. Reinsch, V. Aquilanti, and S. Cavalli, *Phys. Rev. A* **58**, 3718 (1998).
- [29] V. Aquilanti, A. Lombardi, and E. Yurtsever, *Phys. Chem. Chem. Phys.* **4**, 5040 (2002).
- [30] V. Aquilanti, A. Lombardi, M. B. Sevryuk, and E. Yurtsever, *Phys. Rev. Lett.* **93**, 113402 (2004).
- [31] V. Aquilanti, A. Lombardi, and M. B. Sevryuk, *J. Chem. Phys.* **121**, 5579 (2004).
- [32] T. Yanao and K. Takatsuka, *Phys. Rev. A* **68**, 032714 (2003).
- [33] T. Yanao and K. Takatsuka, *J. Chem. Phys.* **120**, 8924 (2004).
- [34] T. Yanao and K. Takatsuka, *Adv. Chem. Phys.* **130 B**, 87 (2005).
- [35] T. Yanao, W. S. Koon, J. E. Marsden, and I. G. Kevrekidis, *J. Chem. Phys.* **126**, 124102 (2007).
- [36] R. S. Berry, *Chem. Rev.* **93**, 2379 (1993).
- [37] P. A. Braier, R. S. Berry, and D. J. Wales, *J. Chem. Phys.* **93**, 8745 (1990).
- [38] T. Komatsuzaki and R. S. Berry, *J. Chem. Phys.* **110**, 9160 (1999); **115**, 4105 (2001).

- [39] J. Jellinek, T. L. Beck, and R. S. Berry, *J. Chem. Phys.* **84**, 2783 (1986).
- [40] H. L. Davis, J. Jellinek, and R. S. Berry, *J. Chem. Phys.* **86**, 6456 (1987).
- [41] P. Labastie and R. L. Whetten, *Phys. Rev. Lett.* **65**, 1567 (1990).
- [42] Y. Zhou, C. K. Hall, and M. Karplus, *Phys. Rev. Lett.* **77**, 2822 (1996).
- [43] M. Takano, T. Takahashi, and K. Nagashima, *Phys. Rev. Lett.* **80**, 5691 (1998).
- [44] G. Strang, *Linear Algebra and its Applications* (Academic Press, New York, 1976).
- [45] N. De Leon, M. A. Mehta, and R. Q. Topper, *J. Chem. Phys.* **94**, 8310 (1991).
- [46] T. Uzer, C. Jaffé, J. Palacián, P. Yanguas, and S. Wiggins, *Nonlinearity* **15**, 957 (2002).
- [47] H. Waalkens, A. Burbanks, and S. Wiggins, *J. Chem. Phys.* **121**, 6207 (2004).
- [48] F. Gabern, W. S. Koon, J. E. Marsden, and S. D. Ross, *Physica D* **211**, 391 (2005).
- [49] C. B. Li, Y. Matsunaga, M. Toda, and T. Komatsuzaki, *J. Chem. Phys.* **123**, 184301 (2005).
- [50] M. Levi, *Physica D* **132**, 150 (1999).
- [51] W. Paul, *Rev. Mod. Phys.* **62**, 531 (1990).
- [52] T. Yanao, W. S. Koon, and J. E. Marsden, *Phys. Rev. A* **73**, 052704 (2006).